A&A 513, A77 (2010)
DOI: 10.1051/0004-6361/200913534

Astronomy & Astrophysics

Anisotropic radiation field and trapped photons around the Kerr black hole *(Research Note)*

R. Takahashi[1] and M. Takahashi[2]

[1] Cosmic Radiation Laboratory, the Institute of Physical and Chemical Research, 2-1 Hirosawa, Wako, Saitama 351-0198, Japan
e-mail: rohta@riken.jp
[2] Department of Physics and Astronomy, Aichi University of Education, Kariya, Aichi 448-8542, Japan
e-mail: takahasi@phyas.aichi-edu.ac.jp

Received 23 October 2009 / Accepted 7 February 2010

ABSTRACT

Aims. In order to understand the anisotropic properties of local radiation field in the curved spacetime around a rotating black hole, we investigate the appearance of a black hole seen by an observer located near the black hole. When the black hole is in front of a source of illumination the black hole casts shadow in the illumination. Accordingly, the appearance of the black hole is called the black hole shadow.

Methods. We first analytically describe the shape of the shadow in terms of constants of motion for a photon seen by the observer in the locally non-rotating reference frame (LNRF). Then, we newly derive the useful equation for the solid angle of the shadow. In a third step, we can easily plot the apparent image of the black hole shadow. Finally, we also calculate the ratio of the photon trapped by the hole and the escape photon to the distant region for photons emitted near the black hole.

Results. From the shape and the size of the black hole shadow, we can understand the signatures of the curved spacetime; i.e., the mass and spin of the black hole. Our equations for the solid angle of the shadow has technical advantages in calculating the photon trapping ratio. That is, this equation is computationally very easy, and gives extremely precise results. This is because this equation is described by the one-parameter integration with given values of the spin and location for the black hole considered. After this, the solid angle can be obtained without numerical calculations of the null geodesics for photons.

Key words. black hole physics – radiative transfer – hydrodynamics – relativity – accretion, accretion disks

1. Introduction

To understand the general relativistic effects on the radiation field around a black hole it is essentially important to elucidate the nature of both the physics and the astrophysics in the curved spacetime. This is because the radiation field plays energetically and dynamically important roles in the accretion flows plunging into the black hole, especially for the supercritical or hypercritical accretion flows, where the photons or neutrinos interact with matter. Even for black holes with low mass accretion rates, the general relativistic effects of the radiation field becomes important because the observational signatures directly reflect the nature of the radiation field. So far, the radiative transfer in curved spacetime was investigated by many authors (e.g. Lindquist 1966; Anderson& Spiegel 1972; Schmid-Burgk 1978; Thorne 1981; Schinder 1988; Turolla & Nobili 1988; Anile & Romano 1992; Cardall & Mezzacappa 2003; Park 2006; Takahashi 2007b, 2008; De Villiers 2008; Farris et al. 2008).

It is believed that the spacetime geometry around a black hole in the real universe is well described by the Kerr metric. In this case, clarifying the effects of the black hole spin on the radiation field is required to understand the nature of the radiation field in the black hole spacetime. Any radiation field around the rotating black hole is influenced by frame-dragging effects, which make an anisotropy of the local radiation field. That is, the anisotropic features of the local radiation field directly reflects the effects of the black hole spin. In the optically thick limit of the radiation field, it is expected that the anisotropy becomes very small (but not zero), because the radiation field and the matter intensely interact. On the other hand, in the optically thin limit of the radiation field the anisotropic nature can be clearly seen in the vicinity of the black hole. For example, for the black holes in the center of the gamma-ray bursts (GRBs) the effects of the neutrino annihilations, which are potentially the energy source of the explosion of the GRB, are well investigated in the optically thin limit of the neutrino radiation field (e.g. Asano & Fukuyama 2001; Miller et al. 2003; Birk et al. 2007). In this case, the black hole's rotation enhances the deposition energy due to the neutrino annihilations. In the optically thin limit, the photons or neutrinos emitted at some location near the black hole are transfered along the null geodesics and some of them are swallowed by the black hole. As is well known, because the propagation rays are influenced by the frame-dragging effects due to the black hole's rotation, at some location near the black hole the effects of the black hole spins are directly seen in the shape and the size of the appearance of the black hole. When a black hole is in front of a source of illumination, the black hole casts a shadow on the illumination. Accordingly, the appearance of the black hole is sometimes called a black hole shadow (e.g. Falcke et al. 2000; Takahashi 2004, 2005; Huang et al. 2007; Bambi & Freese 2009; Hioki & Maeda 2009) or silhouette (e.g. Fukue 2003; Broderick & Loeb 2009; Schee & Stuchlík 2009a). With regard to the realistic accretion flows around black holes, when we observe the black hole with accreting gases, we only see the escape photons emitted by surrounding gases, while the trapped photons make up the shade region.

The observers near the black hole see the black hole shadow in their sky. In this paper we calculate the analytic expression of the shape of the shadow seen by the observer located near the black hole. We also obtain the new equation for the solid angle of the shadow in the sky of the observer. The main purpose of the present study is to show the analytic expressions of the shadow and the equation for the solid angle. Our equation for the solid angle of the shadow has technical advantages. By using this equation, the calculations of the null geodesics around the Kerr spacetime is not required for the calculations of the solid angle. Also, we do not need the particles to be emitted and judge which particles will be swallowed by the black hole, as in the calculations done in e.g. Thorne (1974). Since the equation for the solid angle presented in this paper is described by the one-parameter integration for the given values of the black hole spin and the location, this equation is computationally very easy. We assume $c = 1$ and $G = 1$. After giving some preliminary calculations in Sect. 2, in Sect. 3 we give the analytic expressions for the shape of the shadow seen by the observer near the black hole. In Sect. 4, the equation for the solid angle of the shadow is presented. We give the conclusions in Sect. 5.

2. Preliminaries

2.1. Background metric

We describe the background metric for a Kerr black hole by using the spherical Boyer-Lindquist coordinate. The 3+1 form of the metric $g_{\mu\nu}$ is described as

$$\mathrm{d}s^2 = -\alpha^2\mathrm{d}t^2 + \gamma_{ij}(\mathrm{d}x^i + \beta^i\mathrm{d}t)(\mathrm{d}x^j + \beta^j\mathrm{d}t). \tag{1}$$

On the other hand, the inverse of the metric $g^{\mu\nu}$ is given as

$$g^{\mu\nu}\partial_\mu\partial_\nu = \frac{-1}{\alpha^2}(\partial_t - \beta^i\partial_i)(\partial_t - \beta^j\partial_j) + \gamma^{ij}\partial_i\partial_j. \tag{2}$$

For the Kerr metric described by the spherical Boyer-Lindquist coordinate, the non-zero components of the lapse function (α), the shift vector (β^i and β_i) and the spatial components of the metric (γ_{ij} and γ^{ij}) are given as

$$\alpha = \sqrt{\frac{\Delta\rho^2}{A}}, \quad \beta^\phi = -\omega, \quad \beta_\phi = -\frac{2Mar\sin^2\theta}{\rho^2}, \quad \gamma_{rr} = \frac{\rho^2}{\Delta},$$
$$\gamma_{\theta\theta} = \rho^2, \quad \gamma_{\phi\phi} = \frac{A\sin^2\theta}{\rho^2}, \quad \gamma^{rr} = \frac{\Delta}{\rho^2}, \quad \gamma^{\theta\theta} = \frac{1}{\rho^2}, \quad \gamma^{\phi\phi} = \frac{\rho^2}{A\sin^2\theta}, \tag{3}$$

and $\gamma_{ij} = \gamma^{ij} = 0$ for all other i, j. Here, $\Delta = r^2 - 2Mr + a^2$, $\rho^2 = r^2 + a^2\cos^2\theta$, $A = (r^2 + a^2)^2 - a^2\Delta\sin^2\theta$ and $\omega = 2Mar/A$ and we use $\beta_i = \gamma_{ij}\beta^j$ and $\gamma^{ik}\gamma_{kj} = \delta^i_j$. The determinant of γ_{ij} is given as $\det\gamma_{ij} = \gamma_{rr}\gamma_{\theta\theta}\gamma_{\phi\phi} = (\gamma^{rr}\gamma^{\theta\theta}\gamma^{\phi\phi})^{-1} = A\rho^2\sin^2\theta/\Delta$.

2.2. Locally non-rotating reference frame tetrads

The locally non-rotating reference frame (LNRF) is the frame moving with the four velocity given as $u^\mu = \alpha\delta^\mu_t$. For this frame, the tetrad vectors are given as

$$e^{(0)}_\alpha = [\alpha,\ 0,\ 0,\ 0], \quad e^{(1)}_\alpha = [0,\ \sqrt{\gamma_{rr}},\ 0,\ 0],$$
$$e^{(2)}_\alpha = [0,\ 0,\ \sqrt{\gamma_{\theta\theta}},\ 0], \quad e^{(3)}_\alpha = \sqrt{\gamma_{\phi\phi}}\left[\beta^\phi,\ 0,\ 0,\ 1\right]. \tag{4}$$

In the same way, we have

$$e^\alpha_{(0)} = \frac{1}{\alpha}\left[1,\ 0,\ 0,\ -\beta^\phi\right], \quad e^\alpha_{(1)} = \left[0,\ \sqrt{\gamma^{rr}},\ 0,\ 0\right],$$
$$e^\alpha_{(2)} = \left[0,\ 0,\ \sqrt{\gamma^{\theta\theta}},\ 0\right], \quad e^\alpha_{(3)} = \left[0,\ 0,\ 0,\ \sqrt{\gamma^{\phi\phi}}\right]. \tag{5}$$

2.3. Photon four momentum

The photon four momentum of the photon is calculated from the action S as $p_\alpha = \partial_\alpha S$. The action S is given as

$$S = \frac{1}{2}m^2\lambda - Et + L_z\phi + s_r\int^r\frac{\sqrt{R}}{\Delta}\mathrm{d}r + s_\theta\int^\theta\sqrt{\Theta}\mathrm{d}\theta, \tag{6}$$

where λ is the affine parameter, m is the mass of the particle, E is the energy and L_z is the angular momentum with respect to z-axis. The signs $s_r(=\pm1)$ and $s_\theta(=\pm1)$ correspond to the directions of the propagation of the null geodesics, i.e. the signs of p_r and p_θ determine the signs s_r and s_θ. The functions $\Theta(\theta)$ and $R(r)$ are given as

$$\Theta(\theta) \equiv Q - \cos^2\theta\left(-a^2E^2 + L_z^2/\sin^2\theta\right), \tag{7}$$
$$R(r) \equiv [(r^2 + a^2)E - aL_z]^2 - \Delta\left[(L_z - aE)^2 + Q\right]. \tag{8}$$

Here, Q is the Carter constant. Along the null geodesics, E, L_z and Q are constants of motion. The photon momentum is explicitly given as

$$p_t = \partial_t S = -E, \quad p_\phi = \partial_\phi S = L_z, \quad p_r = \partial_r S = s_r\frac{\sqrt{R}}{\Delta},$$
$$p_\theta = \partial_\theta S = s_\theta\sqrt{\Theta}. \tag{9}$$

Hereafter we newly define

$$r_* \equiv \frac{r}{M}, \quad a_* \equiv \frac{a}{M}, \quad \Delta_* \equiv \frac{\Delta}{M^2} = r_*^2 - 2r_* + a_*^2,$$
$$A_* \equiv \frac{A}{M^4}, \quad \omega_* \equiv \omega M, \quad \rho_*^2 \equiv \frac{\rho^2}{M^2}, \tag{10}$$

and

$$\zeta \equiv \frac{L_z}{ME}, \quad \eta \equiv \frac{Q}{M^2E^2}, \quad R_*(r_*) \equiv \frac{R(r)}{E^2M^4}, \quad \Theta_*(\theta) \equiv \frac{\Theta(\theta)}{M^2E^2}, \tag{11}$$

then we obtain

$$R_*(r_*) = [(r_*^2 + a_*^2) - a_*\zeta]^2 - \Delta_*\left[(\zeta - a_*)^2 + \eta\right], \tag{12}$$
$$\Theta_*(\theta) = \eta + (a_* - \zeta)^2 - (a\sin\theta - \zeta/\sin\theta)^2. \tag{13}$$

Since Θ cannot be negative, there is a constraint of $\eta + (a_* - \zeta)^2 \geq 0$. Now, for $\eta - (a_* - \zeta)^2 = 0$, we have $\sin^2\theta = \zeta/a_*$; that is, $\theta =$ constant. Hereafter, we drop the asterisk of r_* for simplicity. The photon four momentum in the LNRF is calculated as

$$-p^{(t)} = p_{(t)} = \frac{1}{\alpha}(p_t - \beta^\phi p_\phi), \quad p^{(r)} = p_{(r)} = \sqrt{\gamma^{rr}}p_r,$$
$$p^{(\theta)} = p_{(\theta)} = \sqrt{\gamma^{\theta\theta}}p_\theta, \quad p^{(\phi)} = p_{(\phi)} = \sqrt{\gamma^{\phi\phi}}p_\phi. \tag{14}$$

2.4. Innermost unstable orbit

In the motion of the r-direction, the radius of the innermost unstable orbit r_s for a photon is calculated from the equations given as $R_*(r_s) = 0$ and $\partial_{r_s}R_*(r_s) = 0$. From these equations, we have

$$\zeta = \frac{r_s^2 - a_*^2 - r_s\Delta_*(r_s)}{a_*(r_s - 1)}, \quad \eta = \frac{r_s^3}{a_*^2(r_s - 1)^2}\left[4\Delta_*(r_s) - r_s(r_s - 1)^2\right]$$
$$\text{for } a_* \neq 0, \quad \eta + \zeta^2 = 27, \quad r = 3 \quad \text{for } a_* = 0. \tag{15}$$

These results are presented in the past studies (e.g., Bardeen 1973; Chandrasekhar 1983). We note that the innermost unstable orbit was calculated in a different way in the recent study

by Schee & Stuchlík (2009a)[1], in which deeper explanations of the innermost unstable orbit are given (see Sect. 3.3 in Schee & Stuchík 2009a).

3. Shape of the black hole shadow as seen by the locally non-rotating reference frame observer

Here we calculate the shape of the black hole shadow in the sky of the LNRF observer near the black hole. In order to do this, we first introduce the angular coordinates $(\bar{\theta},\ \bar{\phi})$ in the sky of the observer. The direction of the null geodesics passing the observer is described by these coordinates. That is, the photon momentum in the LNRF can be expressed as

$$\begin{aligned} p^{(0)} &= E, \quad p^{(1)} = -E\cos\bar{\theta}, \quad p^{(2)} = E\sin\bar{\theta}\cos\bar{\phi}, \\ p^{(3)} &= E\sin\bar{\theta}\sin\bar{\phi}. \end{aligned} \tag{17}$$

These relations define the angular coordinates $(\bar{\theta},\ \bar{\phi})$. In these definitions, the direction of $\bar{\theta} = 0$ corresponds to the direction of the black hole. Here, we assume

$$[x^{(0)},\ x^{(1)},\ x^{(2)},\ x^{(3)}] = [t,\ r,\ \theta,\ \phi]. \tag{18}$$

In this case, the direction of $p^{(r)}$ corresponds to the angle $\bar{\theta} = \pi$ and the direction of $p^{(\theta)}$ corresponds to $\bar{\phi} = 0$.

On the other hand, by using the LNRF tetrads given above, we have

$$\begin{aligned} \frac{p^{(r)}}{p^{(t)}} &= \frac{s_r\sqrt{R_*/A_*}}{1-\omega_*\zeta}, \quad \frac{p^{(\theta)}}{p^{(t)}} = \left(\frac{\Delta_*}{A_*}\right)^{1/2}\frac{s_\theta\sqrt{\Theta_*}}{1-\omega_*\zeta}, \\ \frac{p^{(\phi)}}{p^{(t)}} &= \left(\frac{\Delta_*^{1/2}\rho_*^2}{A_*\sin\theta}\right)\frac{\zeta}{1-\omega_*\zeta}. \end{aligned} \tag{19}$$

The parameters $(\zeta,\ \eta)$ describing the shape of the black hole shadow are given by Eq. (15) (see, e.g. Bardeen 1973; Chandrasekhar 1983). From the definitions of $(\bar{\theta},\ \bar{\phi})$ in Eq. (17), we have

$$\bar{\theta} = \cos^{-1}\left[-p^{(r)}/p^{(t)}\right], \quad \bar{\phi} = \tan^{-1}\left[\frac{p^{(\phi)}/p^{(t)}}{p^{(\theta)}/p^{(t)}}\right]. \tag{20}$$

With these relations we can specify the position in the sky of the observer from the photon momentum and vice versa. By using Eqs. (19) and (20), we can draw the contour of the black hole shadow in the sky of the observer located at (r,θ). Along the contour of the shadow, we change the parameter r_s of Eq. (15)

[1] In Schee & Stuchlík (2009a), the parameter $\mathcal{L}(=\zeta^2+\eta)$ is used as one of the constants along the geodesics. By using this, the functions $R_*(r_*)$ and $\partial_{r_*}R_*(r_*)$ are related to $\mathcal{L}$ and $\partial_{r_*}\mathcal{L}$ as

$$\begin{aligned} \mathcal{L} &= 2a_*\zeta - a_*^2 + \frac{(r_*^2+a_*^2-a_*\zeta)^2 - R_*}{\Delta_*}, \\ \partial_{r_*}\mathcal{L} &= \frac{2(r_*-1)R_*}{\Delta_*} - \partial_{r_*}R_* + \frac{2(r_*^2+a_*^2-a_*\zeta)}{\Delta_*} \\ &\quad \times\left[2r_*\Delta_* - (r_*-1)(r_*^2+a_*^2-a_*\zeta)\right]. \end{aligned} \tag{16}$$

By using $R_*(r_*) = 0$, $\partial_{r_*}R(r_*) = 0$ and ζ given in Eq. (15), it is shown that $\mathcal{L}_{\rm max} = 0$ and $\partial_{r_*}\mathcal{L}_{\rm max} = 0$. Here, when $R_*(r_*) = 0$, $\mathcal{L} = \mathcal{L}_{\rm max}$ where $\mathcal{L}_{\rm max}$ is given by Eq. (41) in Schee & Stuchlík (2009a). From these calculations we can see that the calculation method for the innermost unstable orbits used in Schee & Stuchlík (2009a) produces the same results in terms of ζ and η as in the past studies of Bardeen (1973) and Chandrasekhar (1983).

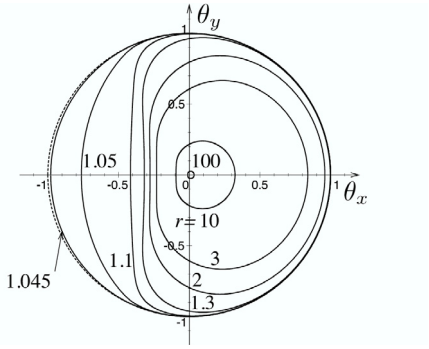

Fig. 1. Shapes of the black hole shadow seen by the observer near the black hole. In this plot, the normalized Lambert map projection described by Eq. (24) is used. The abscissa is θ_x and the ordinate is θ_y. In this figure, the direction of the black hole $(\bar{\theta} = \pi)$ corresponds to $(\theta_x,\ \theta_y) = (0,\ 0)$, and the opposite direction $(\bar{\theta} = 0)$ corresponds to the outermost circle (i.e., $\theta_x^2 + \theta_y^2 = 1$) denoted by the dotted line. The projection of the rotation axis of a black hole corresponds to $\theta_x = 0$. The locations of the observers are $\theta = 85°$ and $r = 100,\ 10,\ 3,\ 2,\ 1.3,\ 1.1,\ 1.05,\ 1.045$. The black hole spin is $a_* = 0.999$. In this case, the radius of the event horizon is $r_+ \sim 1.0447M$.

in the range of $\Theta_* \geq 0$ (see, e.g. Bardeen 1973; Chandrasekhar 1983). Hereafter, we introduce new coordinates

$$X = \sin\bar{\theta}\sin(-\bar{\phi}), \quad Y = \sin\bar{\theta}\cos(-\bar{\phi}), \quad Z = \cos\bar{\theta}. \tag{21}$$

With the coordinates (X, Y, Z), we plot the projection of the black hole shadow onto the sky. This contour is expressed by a closed curve in the sphere (see Fig 2; discussed below). Before doing this, we have to specify the signs of s_r and s_θ. To plot the contour of the shadow, there are two angles of $\Theta(\theta) = 0$, where the sign of s_θ changes across these angles. When the observer is located near the black hole, there are points where the sign of s_r changes. The sign of s_θ is determined by

$$s_\theta = +1 \quad \text{for} \quad Y > 0, \qquad s_\theta = -1 \quad \text{for} \quad Y < 0. \tag{22}$$

On the other hand, when the observer is located far from the black hole, we have $s_r = -1$. This means that all the photons swallowed by the black hole move toward the black hole, i.e. $p^r < 0$. However, when the observer is located near the black hole, even if the photons are emitted in the outgoing direction $p^r > 0$, some of them are swallowed by the black hole. In this case, there are points where the sign of s_r changes in the contours of the shadow. The sign of s_r is determined as

$$s_r = +1 \quad \text{for} \quad \partial_{r_s}R(r) > 0, \qquad s_r = -1 \quad \text{for} \quad \partial_{r_s}R(r) < 0. \tag{23}$$

We note that in $R(r)$, only ζ and η depend on the value of r_s.

The three-dimentional description (X, Y, Z) can be projected with the Lambert map projection (see, e.g. Qihe 2000) given as

$$\begin{cases} \theta_x = k\cos u\sin v \\ \theta_y = k\sin u \end{cases}$$

$$\text{here} \quad k = \sqrt{\frac{2}{1+\cos u\cos v}}, \quad \text{and} \quad \begin{cases} u = \sin^{-1}Y \\ v = \tan^{-1}(X/Z). \end{cases} \tag{24}$$

In Fig. 1, we plot the shapes of the shadows with the normalized Lambert map projection. The abscissa is θ_x and the ordinate is θ_y. In this projection given by Eq. (24), all the area of the sky of the observer is mapped into the region of $\theta_x^2 + \theta_y^2 \leq 1$. In this figure, the direction of the black hole $(\bar{\theta} = \pi)$ corresponds to $(\theta_x,\ \theta_y) = (0,\ 0)$, and the opposite direction $(\bar{\theta} = 0)$ corresponds

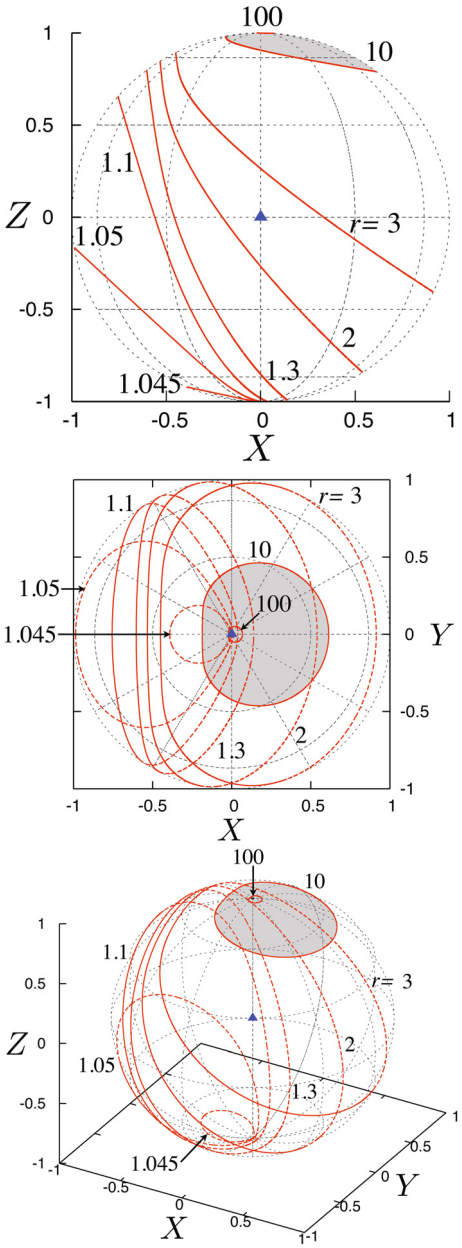

Fig. 2. Black hole shadow in the sky of the observer near the black hole in the three dimensional plot $(X,\ Y,\ Z)$. The parameters are the same as those in Fig. 1. The position of the observer is at the origin $(X, Y, Z) = (0, 0, 0)$ (filled triangles). In the sky of the observer, the direction of the black hole is $(X, Y, Z) = (0, 0, 1)$. The shaded regions are shadows for $r = 10$. The contours of the shadows in the front (opposite) side of the sphere are plotted by the solid (dashed) lines.

to the outermost circle (i.e., $\theta_x^2 + \theta_y^2 = 1$) denoted by the dotted line. Both θ_x and θ_y are normalized so that their maximum values become unity. The location of the observer is $\theta = 85°$ and $r = 100,\ 10,\ 3,\ 2,\ 1.3,\ 1.1,\ 1.05,\ 1.045$. The black hole spin is $a_* = 0.999$. In this case, the radius of the event horizon is $r_+ \sim 1.0447M$. In this figure, the outermost circle denoted by the dotted line is the line of $\bar{\theta} = 0$. As expected, the size of the shadow becomes larger for the observer located closer to the black hole. Interestingly, we can see that some photons in the region of $\theta_x < 0$, can escape to infinity even when the observer is located very near the black hole. This is because of the frame-dragging effect. It is confirmed that no photons emitted at the horizon can escape. In Fig. 2 we plot the projection of the shadows onto the sky in the three dimensional coordinate (X, Y, Z), where the observer is located at the origin, $(X, Y, Z) = (0, 0, 0)$ in this plot (*filled triangles*), and the direction of the black hole is $(X, Y, Z) = (0, 0, 1)$. While most of the photons emitted from the location far from the hole (e.g. $r = 100$) escape to infinity, many of the photons emitted near the black hole are swallowed by the hole (e.g. $r = 1.05$ and 1.045). The parameters are the same as in Fig. 1. The similar signatures seen in Fig. 1 can also be seen in this figure. In Fig. 2, the shadow has a solid angle and its shape is deformed like in Fig. 1. In the next section, we give the new equation for the solid angle.

4. Solid angle for the photons trapped by the black hole

Here we give the equation for the solid angle of the black hole shadow in the sky of the LNRF observer. This solid angle is the function of the black hole spin a_* and the location of the observer (r, θ). When the observer is moving with some velocity, the solid angle also depends on the velocity. Here we only consider the LNRF observer for simplicity. Below we derive first the new equation for the solid angle of the black hole shadow in the sky seen from an observer located at a point near the black hole. Next, we show the distribution of the ratio of the solid angle in the sky in the x-z plane. Note that this ratio corresponds to the ratio of the trapped photon by the hole and the escape photon toward distant regions, when we consider the photons isotropically emitted from a point (as a radiation source in LNRF) near the black hole.

4.1. Equation for the solid angle

The shape of the black hole shadow is symmetric with respect to the Y-Z plane. This makes it sufficient to calculate the solid angles surrounded by the θ_x-axis and the contours of the black hole in the region of $Y \geq 0$. The twice the amount of the solid angle for $Y \geq 0$ corresponds to the amount of the solid angle for the whole region of the black hole shadow. First, we consider the case when the whole region of the black hole shadow exists in the region of $Z \geq 0$, which is the front side of the observer when the observer faces the black hole. In this case, we have $s_r = -1$ and the equations describing the sphere in $Z \geq 0$ are given as

$$Z = (1 - X^2 - Y^2)^{1/2} \equiv f^+(X,\ Y), \tag{25}$$

$$f_X^+ = \frac{-X}{(1 - X^2 - Y^2)^{1/2}}, \quad f_Y^+ = \frac{-Y}{(1 - X^2 - Y^2)^{1/2}}, \tag{26}$$

where f_X and f_Y are the partial derivative of the function f with respect to X and Y, respectively. Now, the solid angle S of the region Ω of the shadow on this sphere is calculated as

$$S = 2 \iint_\Omega \sqrt{(f_X^+)^2 + (f_Y^+)^2 + 1}\, \mathrm{d}X\mathrm{d}Y = 2 \iint_\Omega \frac{\mathrm{d}X\mathrm{d}Y}{\sqrt{1 - X^2 - Y^2}}. \tag{27}$$

Here we introduce the variables $(r,\ \theta)$ as

$$X = r\cos\theta, \quad Y = r\sin\theta. \tag{28}$$

From these definitions, we have

$$r = \sqrt{X^2 + Y^2} = \sin\bar{\theta}, \quad \tan\theta = \frac{Y}{X} = \frac{-1}{\tan\bar{\phi}}, \quad \frac{\partial\theta}{\partial r_s} = \frac{\partial\bar{\phi}}{\partial r_s}. \tag{29}$$

By using these, the solid angle S is calculated as

$$S = 2\iint_\Omega = 2\iint_\Omega \frac{r}{\sqrt{1-r^2}}\mathrm{d}r\mathrm{d}\theta$$
$$= 2\int_0^\pi \mathrm{d}\theta \int_0^{r_{\rm max}(\theta)} \frac{r}{\sqrt{1-r^2}}\mathrm{d}r = 2\int_0^\pi \mathrm{d}\theta\left[1-\sqrt{1-r_{\rm max}^2(\theta)}\right]. \quad (30)$$

Because we now consider the case of $Z \geq 0$, i.e. $0 \leq \bar{\theta} \leq \pi/2$, we obtain

$$\sqrt{1-r_{\rm max}^2(\theta)} = \sqrt{1-\sin^2\bar{\theta}} = \sqrt{\cos^2\bar{\theta}} = \cos\bar{\theta}. \quad (31)$$

Next, by changing the integration variable from θ to r_s, we have the ranges for the integration as follows

$$\theta = 0 \to \pi \text{ and } r_s = r_s^{\rm max} \to r_s^{\rm min}, \quad \text{with} \quad \mathrm{d}\theta = \left(\frac{\partial\theta}{\partial r_s}\right)\mathrm{d}r_s. \quad (32)$$

Then, the solid angle S is given as

$$S = 2\int_{r_s^{\rm min}}^{r_s^{\rm max}} \mathrm{d}r_s \left(-\frac{\partial\bar{\phi}}{\partial r_s}\right)(1-\cos\bar{\theta}), \quad (33)$$

where

$$\cos\bar{\theta} = -s_r\left(\frac{1}{A_*}\right)^{1/2}\frac{\sqrt{R_*}}{1-\omega_*\zeta} \quad (\text{here} \quad s_r = -1). \quad (34)$$

Now we we consider the case where the whole of the black hole shadow exists in the region of $Z \leq 0$ (the back side of the observer). In this case, we have $s_r = -1$ and the equations describing the sphere in $Z \leq 0$ are given as

$$Z = -(1-X^2-Y^2)^{1/2} \equiv f^-(X, Y),$$
$$f_X^- = \frac{X}{(1-X^2-Y^2)^{1/2}}, \quad f_Y^- = \frac{Y}{(1-X^2-Y^2)^{1/2}}. \quad (35)$$

In the same way, we have

$$\sqrt{1-r_{\rm max}^2(\theta)} = \sqrt{1-\sin^2\bar{\theta}} = \sqrt{\cos^2\bar{\theta}} = -\cos\bar{\theta}. \quad (36)$$

The change of the sign of $f^\pm$ do not cause any change because both $f_x^\pm$ and $f_y^\pm$ are used in the form of $(f_x^\pm)^2$ and $(f_y^\pm)^2$, respectively. In terms of the change of the sign before $\cos\bar{\theta}$, this change is canceled out by the change of the sign of s_r. Consequently for the shadow in $Z < 0$ the equation is essentially same as for the shadow in $Z \geq 0$. For the shadow crossing the $Z = 0$, the equation assumes the same form.

In summary, the equation of the solid angle S is given by

$$S = 2\int_{r_s^{\rm min}}^{r_s^{\rm max}} \mathrm{d}r_s\ (-\partial_{r_s}\bar{\phi})\,(1-\cos\bar{\theta}),$$
$$\text{where} \quad \cos\bar{\theta} = -s_r\left(\frac{1}{A_*}\right)^{1/2}\frac{\sqrt{R_*}}{1-\omega_*\zeta},$$
$$\tan\bar{\phi} = \frac{s_\theta\rho_*^2}{A_*^{1/2}\sin\theta}\left(\frac{\zeta}{\sqrt{\Theta_*}}\right). \quad (37)$$

Here the range of the integration for r_s is determined by the condition of $\Theta_* \geq 0$, which can be numerically calculated. Moreover, by using the analytical form for ζ, η, Θ_*, $\bar{\phi}$, $\bar{\theta}$ and so on, the integrand of the integral of Eq. (37) is analytically given as

$$S = -4\rho^2\sin\theta$$
$$\times\int_{r_s^{\rm min}}^{r_s^{\rm max}}\left[\frac{\left(r_s^3-3r_s^2+3r_s-a_*^2\right)\left[r_s^2(r_s-3)\zeta-a_*(r_s-1)\left(\eta+a_*^2\cos^2\theta\right)\right]}{a_*^2(r_s-1)^3(A\sin^2\theta\Theta_*+\rho^4\zeta^2)\sqrt{\Theta_*}}\right.$$
$$\left.\times\left(A^{1/2}+\frac{s_r\sqrt{R_*}}{1-\omega_*\zeta}\right)\right]\mathrm{d}r_s. \quad (38)$$

The derivation of Eq. (38) is given in Appendix A. Equations (37) and (38) are the main results of the present study.

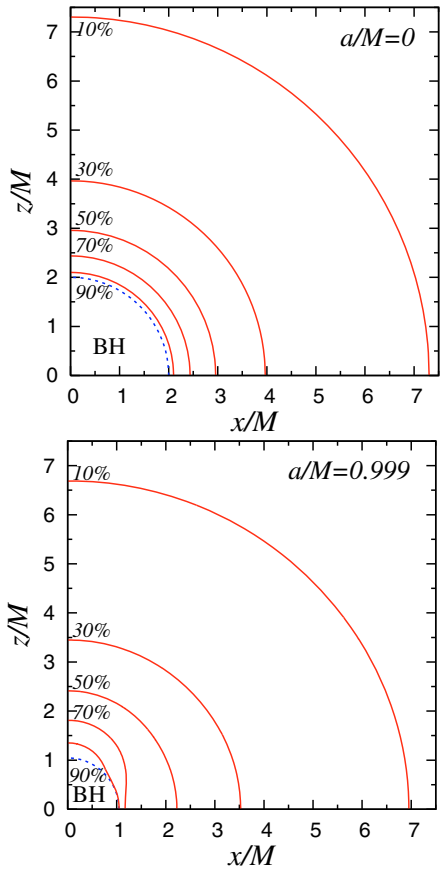

Fig. 3. Photon trapped ratios $S/(4\pi)$ around the black holes with spins of $a_* = 0$ (*top*) and 0.999 (*bottom*). We draw the contours of the trapped ratios for 10%, 30%, 50%, 70%, 90% (solid lines) and the event horizon (dotted lines).

4.2. Photon trapped ratio

Based on Eqs. (37) and (38), we numerically calculate the distribution of the photon trapped ratio $S/(4\pi)$ around the black hole. In Fig. 3 we plot the trapped ratios $S/(4\pi)$ for $a_* = 0$ (*top*) and 0.999 (*bottom*) in the x-z plane. For the rapidly rotating black hole, the photon trapping ratio decreases especially near the equatorial plane because of the frame-dragging effects. That is, the photons near the equatorial plane can escape to infinity more easily than the photons near the pole. These features can also be seen in the shapes of the shadows. Surprisingly, as shown in these plots, 10% to 30% of the photons emitted very close to the black hole (e.g. $r < 1.2$ for $a_* = 0.999$) can escape to infinity. Although these calculations do not take into account the effects of the gravitational redshift, these escaping photons can transport the information of the spacetime and the general

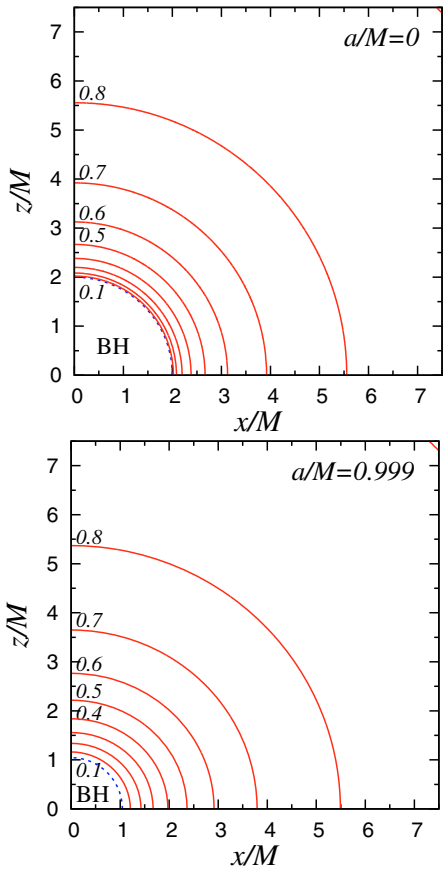

Fig. 4. Lapse function α representing effects of the gravitational redshift for the black holes with spins of $a_* = 0$ (*top*) and 0.999 (*bottom*). We draw the contours of the lapse function for $\alpha = 0.1, 0.2, 0.3, 0.4, 0.5, 0.6, 0.7, 0.8, 0.9$ (solid lines) and the event horizon (dotted lines). We can see the contours for $\alpha = 0.9$ around the regions near $(x/M, z/M) = (0.75,\ 0.75)$ in both panels. At the event horizon the value of α becomes zero.

relativistic phenomena to the observer at infinity. These results about the trapped ratio for photons are very important when we consider the radiative phenomena that arise near the event horizon. In Fig. 4 we plot the lapse function α representing the effects of gravitational redshift for black hole spins of $a/M = 0$ (*top*) and 0.9 (*bottom*). The contours of the lapse function in Fig. 4 shows nearly spherical shapes, which is contrast to the plots of the photon trapped ratios in Fig. 3. Then, even if we take the effects of the gravitational redshift into account, the energy amount of the escaping photons near the equatorial plane is than that near the pole region for the case of the rapidly rotating black hole.

5. Discussion and conclusions

Since the last century, observational data containing information of the black hole spacetime have been obtained for the black hole candidates in e.g. the active galactic nuclei, the X-ray black-hole binaries and the Galactic center of our galaxy. However, the parameters of the black hole spacetime like mass and spin estimated in the past studies usually and highly depend on the assumed accretion flow models, and so far the final values of the parameters of the black hole, especially the black hole spin, have not been obtained for any black hole candidates. This is because the observational data usually contain the information of the plasma physics of the accreting matter in addition to the information of the spacetime metric, and frequently both these informations (metric and plasma physics) are degenerate in the observational data. In these cases we cannot uniquely determine the spacetime metric from the observational data. Because the optical phenomena directly reflect the spacetime metric, the spacetime metric can be uniquely determined if the observational signatures closely related to the optical phenomena like the contours of the black hole shadow can be found in the observational data. For this purpose a deep understanding of the optical phenomena around the black hole is important.

In past studies it was proposed that the black hole's metric can be estimated from the observational features like the line and continuum spectrum, quasi-periodic oscillation (QPO), radio visibility, polarization (see, reviews, e.g., Remillard & McClintock 2006; Psaltis 2008). However, all these observational signatures highly depend on the accretion flow models. Actually, for some black hole candidates, several values of the black hole spin can be proposed for one and the same black hole candidate. For example, in terms of the iron line spectrum observed in an X-ray black hole binary, it is pointed out that the Fe K line profile and the estimated value of the black hole spin of the black hole binary GX 339-4 highly depend on the assumed continuum spectrum, which is first subtracted from the observational data to make the line profile (Yamada et al. 2009). This means that the black hole spin cannot be correctly estimated from the line profile unless we can uniquely determine the accretion flow model, which produces the continuum spectrum. On the other hand, in terms of the observed QPO phenomena, the origin of the QPO is still under debate, although some theoretical models of the QPO like the disk oscillation model have been proposed. In terms of X-ray polarization of the accretion disk, the observed polarization features highly depend on the corona models. However, we do not fully understand the production mechanism and physical properties like the spatial distribution of the corona. Therefore, to understand the observational signatures containing the information of the spacetime, the physics of the accretion flows and outflows (and/or jets) around the black holes should be deeply investigated and understood especially by means of magnetohydrodynamic simulations with effects of the radiation fields. Actually, recently magnetohydrodynamic simulations with effects of the radiation are attempted (e.g. De Villiers 2008; Farris et al. 2008; Mościbrodzka et al. 2009). In the near future, the radiation fields around the black hole spacetime will be exactly solved by the dynamical simulations with effects of the anisotropy of the radiation field considered in this paper. Because the equation given in this study provide the exact results of the contours of the black hole shadow and the photon trapped ratio, the equation given in this study can be used for the code tests in the developments of simulation code of the radiation field.

We have the appearance of the black hole (the black hole shadow) seen by the observer located near the black hole. In summary the calculation method for the photon trapped ratio presented in this study can be extended to the astropysically more plausible cases. Although in this study we assume the LNRF, the calculation in this study can be extended to other reference frames moving with astrophysically frequently considered velocity fields like corotating or counterrotating Keplerian disks. Actually, in the past studies, other frames like a static frame, a circular geodesic frame (or a Keplerian frame) and a radially falling frame considered (e.g. Takahashi 2007a; Schee & Stuchlík 2009a,b) in addition to the LNRF. Especially Schee & Stuchlík (2009a) gave the equation and contours of the black hole silhouettes by using these frames. In addition to the

contours, the equation of the photon trapping ratio presented in this study (Eqs. (37) and (38)) can be straightforwardly extended to a more general velocity field.

Acknowledgements. R.T. is grateful to Professors K. Makishima, Y. Eriguchi and S. Mineshige for their continuous encouragements, and to K. Ohsuga, Y. Kato, J. Fukue, Y. Sekiguchi for useful discussion. The authors thank the referee, Prof. Z. Stuchlík, for valuable comments and suggestions, which improved the original manuscript. This research is supported by the Grant-in-Aid for Scientific Research Fund of the Ministry of Education, Culture, Sports, Science and Technology, Japan [Young Scientists (B) 21740149 (RT)].

Appendix A: Derivation of Eq. (38)

First, we give the analytic expression for the partial derivative $\partial\bar{\phi}/\partial r_s$ appeared in Eq. (37). Both η and ζ are the function of r_s calculated as

$$\begin{aligned}\zeta &= \frac{-1}{a_*(r_s-1)}(r_s^3-3r_s^2+a_*^2r_s+a_*^2),\\ \eta &= \frac{-r_s^3}{a_*^2(r_s-1)^2}(r_s^3-6r_s^2+9r_s-4a_*^2).\end{aligned} \tag{A.1}$$

Based on this, the derivatives of these with respect to r_s is analytically calculated as

$$\begin{aligned}(\partial_{r_s}\zeta) &= \frac{-2}{a_*(r_s-1)^2}(r_s^3-3r_s^2+3r_s-a_*^2),\\ (\partial_{r_s}\eta) &= \frac{-4r_s^2(r_s-3)}{a_*^2(r_s-1)^3}(r_s^3-3r_s^2+3r_s-a_*^2).\end{aligned} \tag{A.2}$$

From Eq. (A.2), we know the relation of

$$(\partial_{r_s}\eta) = \frac{2r_s^2(r_s-3)}{a_*(r_s-1)}(\partial_{r_s}\zeta). \tag{A.3}$$

On the other hand, the partial derivative of Θ_* with respect to r_s is given as

$$(\partial_{r_s}\Theta_*) = -\frac{2\zeta}{\tan^2\theta}(\partial_{r_s}\zeta)+(\partial_{r_s}\eta), \quad (\partial_{r_s}\sqrt{\Theta_*}) = \frac{\partial_{r_s}\Theta_*}{2\sqrt{\Theta_*}}, \tag{A.4}$$

if we introduce

$$\begin{aligned}n^{(x)} &\equiv \frac{p^{(\theta)}}{p^{(t)}} = \sin\bar{\theta}\cos\bar{\phi}, \quad n^{(y)} \equiv \frac{p^{(\phi)}}{p^{(t)}} = \sin\bar{\theta}\sin\bar{\phi},\\ n^{(z)} &\equiv -\frac{p^{(r)}}{p^{(t)}} = \cos\bar{\theta},\end{aligned} \tag{A.5}$$

and

$$n^{(w)} \equiv \frac{n^{(y)}}{n^{(x)}} = \tan\bar{\phi} = \frac{s_\theta\rho^2}{A^{1/2}\sin\theta}\left(\frac{\zeta}{\sqrt{\Theta}}\right), \tag{A.6}$$

we have

$$\partial_{r_s}\bar{\phi} = \cos^2\bar{\phi}\,(\partial_{r_s}n^{(w)}) \tag{A.7}$$

$$= \frac{1}{1+(n^w)^2}\left(\frac{s_\theta\rho^2}{A^{1/2}\sin\theta}\right)\partial_{r_s}\left(\frac{\zeta}{\sqrt{\Theta}}\right) \tag{A.8}$$

$$= \frac{s_\theta A^{1/2}\rho^2\sin\theta}{2\sqrt{\Theta_*}(A\sin^2\theta\Theta_*+\rho^4\zeta^2)} \times\left[2(\eta+a_*^2\cos^2\theta)(\partial_{r_s}\zeta)-\zeta(\partial_{r_s}\eta)\right]. \tag{A.9}$$

On the other hand, the factor $1-\cos\bar{\theta}$ in the integral given in Eq. (37) is calculated as

$$1-\cos\bar{\theta} = 1+\left(\frac{s_r}{A^{1/2}}\right)\frac{\sqrt{R_*}}{1-\omega_*\zeta}. \tag{A.10}$$

By using the analytic expressions for $\partial_{r_s}\bar{\phi}$ and $1-\cos\bar{\theta}$, the solid angle S is calculated as

$$S = 2\int_{r_s^{\rm min}}^{r_s^{\rm max}} dr_s \frac{A^{1/2}\rho^2\sin\theta}{2\sqrt{\Theta_*}(A\sin^2\theta\Theta_*+\rho^4\zeta^2)}\Big[\zeta(\partial_{r_s}\eta) -2(\eta+a_*^2\cos^2\theta)(\partial_{r_s}\zeta)\Big]\left[1+\left(\frac{s_r}{A^{1/2}}\right)\frac{\sqrt{R_*}}{1-\omega_*\zeta}\right] \tag{A.11}$$

$$= 2\rho^2\sin\theta\int_{r_s^{\rm min}}^{r_s^{\rm max}} dr_s \frac{(\partial_{r_s}\zeta)}{\sqrt{\Theta_*}(A\sin^2\theta\Theta_*+\rho^4\zeta^2)}\left[\frac{r_s^2(r_s-3)}{a_*(r_s-1)}\zeta -\eta-a_*^2\cos^2\theta\right]\left(A^{1/2}+\frac{s_r\sqrt{R_*}}{1-\omega_*\zeta}\right) \tag{A.12}$$

$$= -4\rho^2\sin\theta \times\int_{r_s^{\rm min}}^{r_s^{\rm max}} \frac{\left(r_s^3-3r_s^2+3r_s-a_*^2\right)\left[r_s^2(r_s-3)\zeta-a_*(r_s-1)\left(\eta+a_*^2\cos^2\theta\right)\right]}{a_*^2(r_s-1)^3(A\sin^2\theta\Theta_*+\rho^4\zeta^2)\sqrt{\Theta_*}} \times\left(A^{1/2}+\frac{s_r\sqrt{R_*}}{1-\omega_*\zeta}\right)dr_s, \tag{A.13}$$

where the analytic expressions for ζ, η, Θ_* and R_* are given above.

References

Anile, A. M., & Romano V. 1992, ApJ, 386, 325
Anderson, J. L., & Spiegel, E. A. 1972, ApJ, 171, 127
Asano, K., & Fukuyama, T. 2001, ApJ, 546, 1019
Bardeen, J. M. 1973, in Black Holes, ed. C. DeWitt, & B. S. DeWitt (New York: Gordon and Breach), 215
Bambi, C., & Freese, K. 2009, Phys. Rev. D, 79, 043002
Birkl, R., Aloy, M. A., Janka, H.-Th., & Müller, E. 2007, A&A, 463, 51
Broderick, A. E., & Loeb, A. 2009, ApJ, 697, 1164
Chandrasekhar, S. 1983, The Mathematical Theory of Black Holes (Oxford: Clarendon)
Cardall, C. Y., & Mezzacappa, A. 2003, Phys. Rev. D, 68, 023006
De Villiers, J.-P. 2008, unpublished [arXiv:0802.0848]
Falcke, H., Melia, F., & Agol, E. 2000, ApJ, 528, L13
Farris, B. D., Li, T. K., Liu, Y. T., & Shapiro, S. L. 2008, Phys. Rev. D, 78, 024023
Fukue, J. 2003, PASJ, 55, 155
Hioki, K., & Maeda, K. 2009, Phys. Rev. D, 80, 024042
Huang, L., Cai, M., Shen, Z.-Q., & Yuan, F. 2007, MNRAS, 379, 833
Kneller, J. P., McLaughlin, G. C., & Surman, R. A. 2006, J. Phys. G: Nucl. Part. Phys., 32, 443
Lindquist, R. W. 1966, Ann. Phys., 37, 487
Mihalas, D. 1980, ApJ, 237, 574
Miller, W. A., George, N. D., Khefets, A., & McGhee, J. M. 2003, ApJ, 583, 833
Misner, C. W., Thorne, K. S., & Wheeler, J. A. 1973, Gravitation (Freeman)
Mościbrodzka, M., Gammie, C. F., Dolence, J. C., Shiokawa, H., & Leung, P. K. 2009, ApJ, 706, 497
Park, M.-G. 1993, A&A, 274, 642
Park, M.-G. 2006, MNRAS, 367, 1739
Psaltis, D. 2008, Liv. Rev. Relativ., 11, 9
Qihe, H. Y., John, P. S., & Waldo, R. T. 2000, Map projection transformation: principles and applications (New York: Taylor & Francis)
Remillard, R. A., & McClintock, J. E. 2006, ARA&A, 44, 49
Schmid-Burgk, J. 1978, Ap&SS, 56, 191
Schinder, P.-J., & Bludman, S. A. 1989, ApJ, 346, 350
Schee, J., & Stuchlík, Z. 2009a, Int. J. Mod. Phys. D, 18, 983
Schee, J., & Stuchlík, Z. 2009b, Gen. Relativ. Grait., 41, 1795
Takahashi, R. 2004, ApJ, 611, 996
Takahashi, R. 2005, PASJ, 57, 273
Takahashi, R. 2007a, MNRAS, 382, 567
Takahashi, R. 2007b, MNRAS, 382, 1041
Takahashi, R. 2008, MNRAS, 383, 1155
Thorne, K. S. 1974, ApJ, 191, 507
Thorne, K. S. 1981, MNRAS, 194, 439
Turolla, R., & Nobili, L. 1988, MNRAS, 235, 1273
Yamada, S., Makishina, K. Uehara, Y., et al. 2009, ApJ, 707, L109